Acta Materialia 103 (2016) 754–760

Contents lists available at ScienceDirect

Acta Materialia

journal homepage: www.elsevier.com/locate/actamat

Full length article

Grain boundary segregation in binary nickel–bismuth alloy

M.R. Chellali [a, b, c, *], L. Zheng [c, d], R. Schlesiger [c], B. Bakhti [e], A. Hamou [b], J. Janovec [a], G. Schmitz [f]

[a] Slovak University of Technology in Bratislava, Faculty of Materials Science and Technology in Trnava, Paulinska 16, 917 24 Trnava, Slovakia
[b] Laboratory of Environmental Science and Material Studies, University of Oran 1-Ahmed Benbella, Oran, Algeria
[c] Institute of Materials Physics, University of Münster, Wilhelm-Klemm-Str. 10, D-48149 Münster, Germany
[d] University of Science and Technology Beijing, School of Materials Science and Engineering, 100083 Beijing, China
[e] Fachbereich Physik, Universität Osnabrück, D-49076 Osnabrück, Germany
[f] Institute of Materials Science, University of Stuttgart, Heisenbergstraße 3, Stuttgart D-70569, Germany

ARTICLE INFO

Article history:
Received 11 August 2015
Received in revised form
10 October 2015
Accepted 3 November 2015
Available online xxx

Keywords:
Nickel
Bismuth
Grain-boundary segregation
Embrittlement
Atom probe tomography
Nanocrystalline alloys

ABSTRACT

Grain boundary segregation and segregation kinetics are investigated by means of atom probe tomography in a binary Nanocrystalline nickel-bismuth alloy. Gibbsian excess and width of segregation layers at grain boundary are quantitatively determined. If segregation is approximated by McLean kinetics, remarkably fast volume transport of bismuth is derived. However, details of the segregation kinetics are in significant contrast to the McLean model. Additional influence of attractive Bismuth interaction is indicated. The experimentally demonstrated clear segregation tendency suggests that reported embrittlement of Ni–Bi alloys is due to significant grain boundary segregation of Bi. Diffusivity of Bi in nanocrystalline Ni and segregation amplitude were found to be$D_B \approx (2.16 \pm 0.48) \times 10^{-21}$ m^{2}s^{-1}, and 17 respectively.

1. Introduction

Nickel (Ni) based alloys are advanced structural materials that are mainly used in aircraft engines but are also applied in the chemical, petrochemical and electrical industries [1,2]. Because of their undesired embrittlement at intermediate temperatures, these alloys were already subject of extended studies [3–6]. Many researchers [7,8] considered the intermediate temperature embrittlement (ITE) of Ni-based superalloys to be caused by the evolution of intergranular precipitates. However, several experiments demonstrated that commercially pure or only weakly alloyed Ni also show evident ITE [9,10]. In this case, the interpretation of intergranular precipitates is doubtful. Alternatively, it has been suggested that this embrittlement is related to equilibrium grain boundary (GB) segregation [11], or possibly even kinetically driven non-equilibrium segregation [12,13].

GB segregation is the enrichment of GBs by impurity atoms during an annealing treatment. Because of a strong segregation tendency, even very small amounts of antimony, phosphorus, tin, or sulphur can cause an undesired embrittlement in iron and nickel based alloys [14]. On the other hand, small amounts of boron, molybdenum at GBs can increase the ductility of steels [15]. Interfacial chemistry also affects mobility, GB energy, and the stability of nanostructures [16,17]. Local solute decoration may lead to the nucleation of second phases, creation of complexions [18], or choosy melting of GBs [19]. Moreover, semiconductors are distressed by GB segregation owing to band structure fluctuations that alter the recombination motion of charge carriers [20]. The study of Copper (Cu) embrittlement by GB segregation of Bismuth (Bi) has a long history [21,22]. However, the Ni(Bi) is also an interesting system, due to its phase diagram similarity with binary Cu(Bi) alloy and because of its vast industrial application [23,24]. In a previous article [13] we had proven, that, while high purity Ni shows no ITE, even an amount as small as 25 wt ppm of Bi is sufficient to produce the well know ductility loss at intermediate temperatures (see Fig. 1).

Despite its massive industrial application, segregation and transport data are mostly lacking for the Ni–Bi system. GB

* Corresponding author. Slovak University of Technology in Bratislava, Faculty of Materials Science and Technology in Trnava, Paulinska 16, 917 24 Trnava, Slovakia.
E-mail address: m_chel01@uni-muenster.de (M.R. Chellali).

http://dx.doi.org/10.1016/j.actamat.2015.11.003
1359-6454/

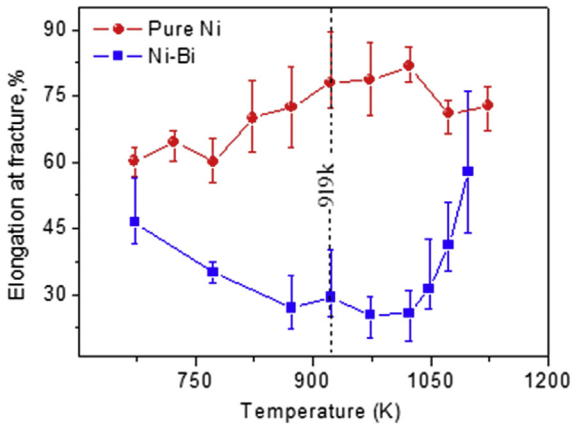

Fig. 1. Maximum elongation of high purity Ni and a Ni-25ppm-Bi alloy versus temperature of mechanical testing (Error bars display the maximum and minimum elongations of six samples with identical heat treatment and tension procedure). Maximum temperature (915 K) of stable intermetallic is indicated.

segregation was investigated using Auger electron spectroscopy by Chang and Huang [11]. However, reported segregation enthalpy exceeding 100 kJ/mol makes it worth to conduct complementing experiments to determine fundamental thermodynamic parameters using different, probably more accurate methods. Therefore in this article, we will present a study by atom probe tomography (APT) on GB segregation and related atomic transport in the Ni–Bi system. The instrument enables real three-dimensional chemical maps of the specimen in atomic resolution, which allows direct analysis of inclined GBs embedded into bulk volume. Individual atoms of the specimen are field-evaporated by short high voltage pulses, of up to 5 kV, superimposed on a constant bias voltage a few times larger than the pulse voltage itself. Evaporated atoms are accelerated towards a detector that records flight time and impact position. From data of detector events, the three-dimensional atomic arrangement of the specimen can be reconstructed with an accuracy of a few Angstroms [25]. As a decisive advantage, atom probe tomography does not require fracture of GBs to discover segregation. It allows direct local measurement of individual GB and to determine spatial distribution of the segregation zone.

2. Materials and methods

We investigated GBs of Ni-25wt ppm-Bi produced by vacuum induction melting, mixing high-purity Ni with the correct amount of high-purity Bi. The morphologies of the alloys were observed by scanning electron microscopy (SEM, FEI Nova 230 Nano). Furthermore, the samples were thinned to <100 nm thick with ZEISS Cross-Beam 1540 EsB focussed ion beam system (FIB), lifted-out and cut by Gallium (Ga) ions. The atomic structure was performed by high-resolution transmission electron microscopy (HRTEM) model Zeiss Libra 200F.

Analysis was also carried out using a modern wide angle tomographic atom probe (WATAP). Base and pulse voltage are optimized for single atom detection (detection rate<0.05 atoms/pulse). The instrument is equipped with a 120 mm delay line detector and a flight length of 150 mm, which results in a numerical aperture of ±35°. Therefore, lateral size of the analyzed volume has been increased up to typically 100 nm in diameter. This allows measurement of rare defects with sufficient statistically significance [26,27]. Samples were evaporated by high voltage pulsing at a pulse rate of 20 kHz, a pulse fraction $U_{Pulse}/U_{DC} = 20\%$ and a specimen temperature of 80 K.

In order to obtain sufficient sample throughput for a kinetic study, which requires investigation of many samples in different reaction stages, we decided to deposit model layers on pre-shaped tungsten tips. Nanocrystalline ($Ni_{97}Bi_3$) alloy layers of about 25 nm thickness were deposited using a custom-built ion beam sputter device. An additional very thin Al layer was deposited on top of the coated specimens to avoid evaporation of Bi during subsequent heat treatments.

Coated tips were annealed in an ultra-high vacuum (UHV) furnace with a residual gas pressure below 1×10^{-7} mbar to induce Bi segregation to the grain boundaries. Annealing temperature was 623 K, annealing times varied from 15 to 120 min. The temperature of the tips inside the vacuum furnace was carefully calibrated against the melting point of high purity (99.998 wt%) Sn wires. Possible deviations between the measured and real temperatures of the nanometric tip are proven to be less than ±10 K in studied temperature regime.

Thin film deposition on curved substrates leads to significantly smaller grain size (in the range of 10 nm) in comparison to conventional industrial alloys. In order to compensate for the dramatically increased volume fraction of grain boundaries, the Bi content was increased to 3 at% in our model layers. This impurity content is certainly above the solubility limit for Bi in Ni [28]. As a decisive advantage, small grains improve the frequency of finding suitable GBs in the analyzed volume [29,30].

3. Results

Fig. 2(a) presents the SEM image of the binary Ni(Bi) alloy. Grains, GBs and triple junctions (TJ) are clearly seen. No intergranular precipitates in the size of submicrometers are shown. From the inset of the Fig. 2(a), the presence of a GB within the lamella can be identified by contrast of two grains. Fig. 2(b) shows TEM images of the lamella with emphasis on grain boundary as bright-field and high resolution electron microscopy (HREM) images respectively. No precipitation is formed at GBs.

Fig. 3(a) presents a mass spectrum obtained by APT-analysis of the sputter-deposited alloy layer with nominal 3 at% Bi in the as-prepared state. All major peaks are clearly identified and by virtue of their disparate atomic weights, no peak overlap is observed between Ni and Bi. Determined average concentration of Bi is close to the expected 3%, no systematic variation of the total Bi content is noticed with annealing time (see the table in the inset of Fig. 3(b)). Thus, potential Bi loss due to high vapor pressure is reliably prevented by Al coating.

Fig. 4 presents the compositional analysis of different annealing stages. Cross section through the atomic reconstruction and composition profile of the as prepared state (Fig. 4(a)) demonstrate a homogeneous Bi distribution. After annealing, enrichment of Bi at GBs of Ni is evident (see e.g. inset of Fig. 4(c). The complex 3D morphology of the GBs becomes nicely decorated by Bi markers. In order to analyze grain boundaries after annealing, local cylinders of analysis are oriented perpendicular to GBs and the corresponding concentration profiles are determined across the grain boundaries. Always, the cylinder orientation is optimized to reveal a chemical transition as sharp as possible, cylinder diameter was 6 nm. Examples of GB cross section profiles obtained after 15, 30 and 45 min annealing at 623 K are presented in Fig 4(b–d). Peak GB concentration reaches 9.8, 20.6 and 27.6 at% Bi, respectively. Also the width (w) of the segregation zone increases clearly with time.

Since width of segregation zones varies, it is obviously not sufficient to determine the peak composition to characterize the progress of segregation. A more robust parameter is the Gibbsian excess Γ that counts the number of additional Bi atoms per GB area. If tomographic reconstructions are evaluated in the vicinity to GBs,

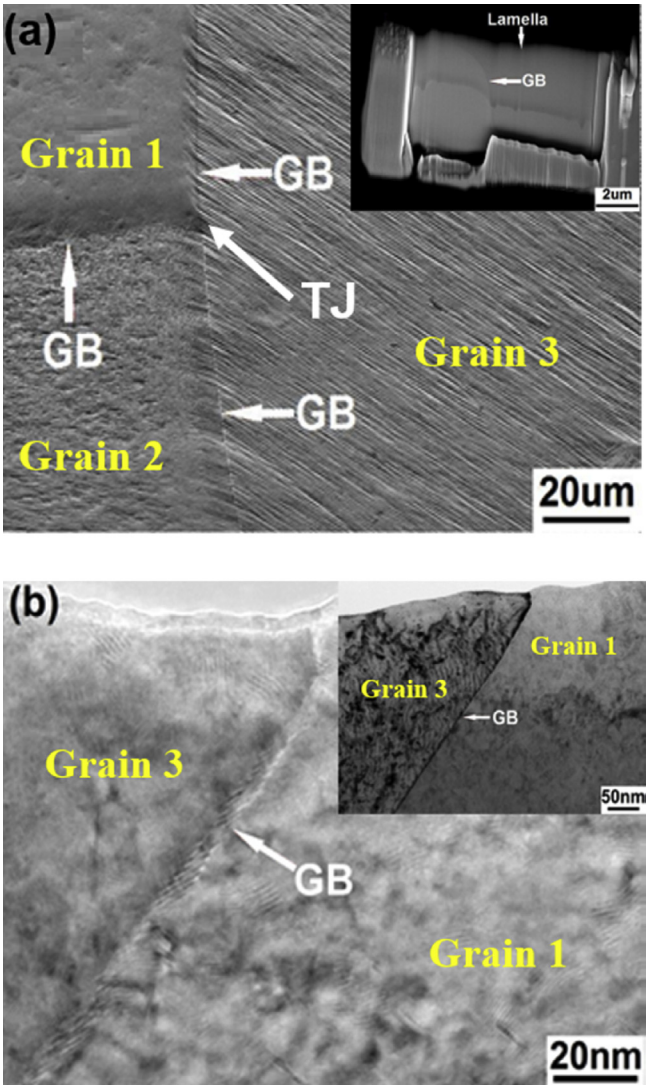

Fig. 2. Electron microscope images of Ni–Bi alloys with emphasis on grain boundary (GB) and triple junction (TJ). (a) SEM image. (b) HREM image. Insets show: procedures of preparing a lamella for TEM observation by FIB (a) and bright field image (b). The samples are heat-treated at 1023 K for 45 min.

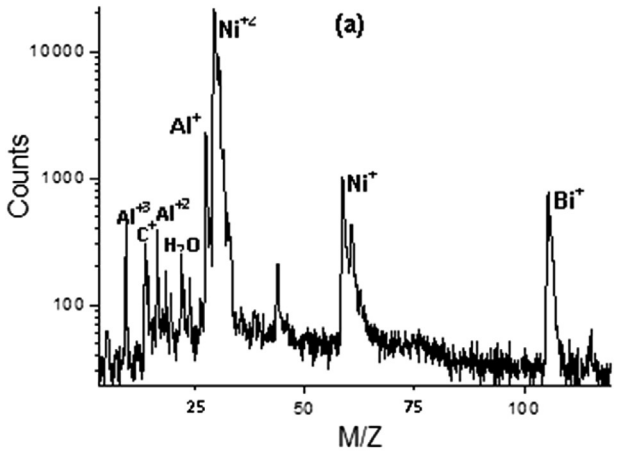

(b)

Annealing time (min)	Bi Concentration (at. %)
0 min	(2.96± 0.04)
15 min	(2.93 ± 0.05)
30 min	(2.87 ± 0.1)
45 min	(2.73 ± 0.08)
90 min	(2.45 ± 0.15)
120 min	(2.39 ± 0.11)

Fig. 3. APT measurements of as-prepared state: Mass spectrum of a Ni-3at%–Bi sample, in the as-prepared state. Inset table presents total Bi concentration at different annealing states.

we frequently notice local density variations. Interestingly, we do observe increase of density as well as depletion. Until now, we could not identify an unambiguous correlation of this effect to grain orientation relation. In any case however, this density variation prevents simple determination of the Gibbsian excess from determined composition profiles. Instead, we generate ladder diagrams from the atomic data comprised in the analysis cylinder in the same way as in the Fig. 4. While continuously increasing the cylinder length, we plot the number of Bi atoms versus the total number of atoms (see Fig. 5). The slopes on the left and right hand side of this graph represent the concentrations of Bi in the grain volume. Gibbsian excess is determined as the shift between appropriate tangents.

The Gibbs-excess in units of Bi monolayers (and atoms/cm^2) and for comparison the Bi content of grain volume as they were observed during isothermal heat treatment at 623 K are plotted versus annealing time in Figs. 6(a) and (b), respectively. Table 1 summarizes the quantitative results.

Observed variation of density is an indicator for the influence of methodical artefacts. Since possible effects of local magnification are expected to depend on the inclination of the GB relative to tip axis, we also plot in Fig. 7 the angular dependencies of GB width and peak concentration for the stage after 15 min annealing. Averaged on several individual grain boundaries, variation is seen to be close to the statistical error of averaging. So, a significant effect by local magnification or erroneous calibration of the aspect ratio in length scales can be probably ruled out.

4. Discussion

Fig. 2 shows that no precipitates within grains, GBs or in TJs were found in specimens' heat treated at 1023 K. This is in accordance with the Ni–Bi phase diagram, which predicts no intermetallic phases above 919 K. However, our mechanical tests have shown a clear ductility loss at this temperature (see the dashed line in Fig. 1). Indeed, the ductility minimum is well above the possible existence temperature of the intermetallic phases. This indicates that GB precipitation does not cause the evident ITE in the Ni–Bi alloy. Miskovic [10], investigated the vacuum cast nickel base IN 939 in the as cast condition, as well as in the fully heat treated condition. Measurements showed a ductility minimum at 1073 K for the as-cast condition while no ITE was found for the fully heat treated condition. He et al. [3] found that a ductility minimum of Ni-based superalloys M963 was observed at 1073 K under solution treatment and disappeared under age treatment. Besides, Sharghi [31] found the minimum ductility of IN-738LC superalloys in standard heat treatment condition at 923 K. However, no drop in ductility was observed for samples aged heated for longer annealing times. In 2009, the tensile properties of Ni-based superalloys

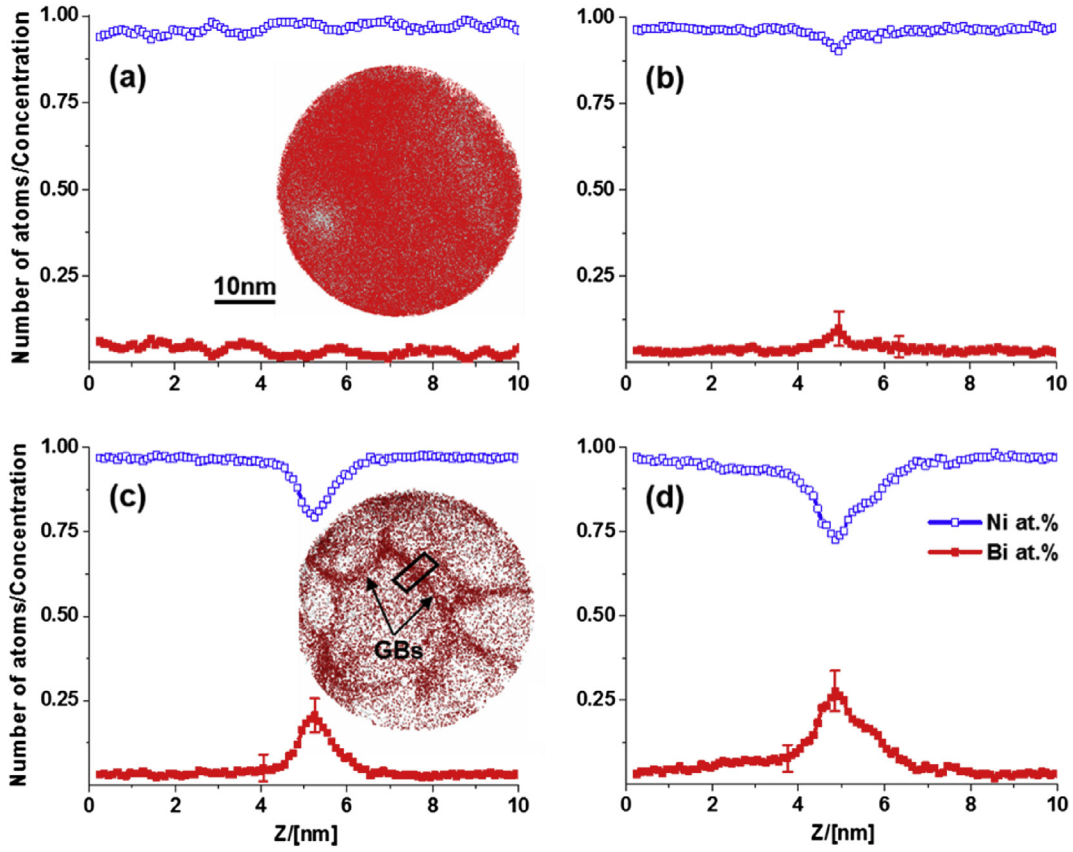

Fig. 4. Compositional analysis of Bismuth in Nanocrystalline Ni: a) arbitrary volume of as-prepared state. b), c) and d) represent concentration profiles across GB after 15, 30 and 45 min annealing at 623 K, respectively (error bars mark 1σ range). Insets show: Atomic reconstruction of Ni(Bi) alloy (only Bi atoms are shown) in the as-prepared state(a) and after 30 min annealing at 623 K (c). In the latter, segregation of Bi to GBs of Ni becomes obvious).

720Li were measured by Gopinath et al. [32]. Consequently, no ITE after two stages of long time aging was observed. Thus, the most suitable candidate to explain this phenomenon in Ni and Ni-based superalloys is GB segregation, either equilibrium or non-equilibrium.

As evident from Fig. 6(a), a pronounced segregation of Bi to GBs in the Nanocrystalline Ni-3at.%Bi model alloy, is clearly proven by atom probe analysis. During annealing at 623 K, GBs segregation grows with time, but assumes a finite saturation level after about 90 min. Observed monotonous increase towards saturation points at a thermodynamic origin with a well-defined equilibrium segregation factor. Comparison between the Gibbsian excess (Fig. 6(a)) and the remaining volume content of Bi (Fig. 6(b)) allows an independent check of applied procedure to determine the GB excess. It can be clearly seen that Segregation of Bi is increasing in GBs and decreasing in grains volume (see Fig. 6). Since total amount of Bi is practically constant (see Fig. 3(b)), segregation at GBs and remaining concentration in the grain volume are correlated as:

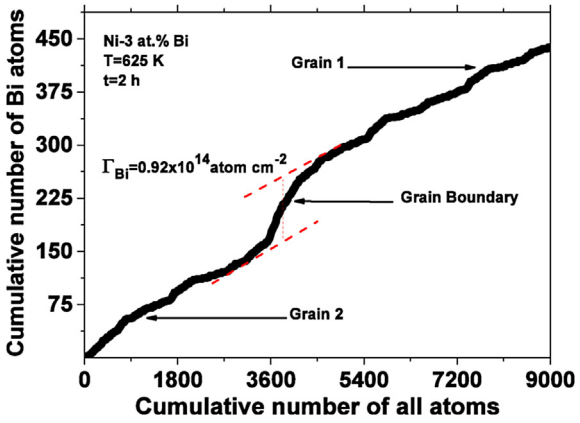

Fig. 5. Integral profile of detected atoms and density of bismuth as function of depth within the cylinder across GB.

$$C_B(t) = C_0 - \frac{3\Omega}{d} \cdot \Gamma(t) \quad (1)$$

C_B, C_0, Ω, Γ and d denote actual and initial Bi concentration in bulk, average atomic volume, Gibbsian excess, and grain diameter, respectively. As demonstrated in Fig. 6(b), the measured concentrations (Black diamonds) and the calculated data sets (red squares) are well compatible, if spherical grains of 10 nm average diameter are assumed. The proposed structure corresponds well with the mean grain size of the material ($d = 13$ nm) (see e.g. Fig. 4(c)). Thus it is concluded, that also in this early state Bi is already segregated favorably in the grain boundaries.

The detailed characterization by atom probe analysis makes obvious three important points:

i) Segregated atoms occupy a zone of finite thickness around the GBs which is definitely broader than the structural width of the GB and which furthermore depends on the total amount of segregated atoms. Thus, a future atom probe study under

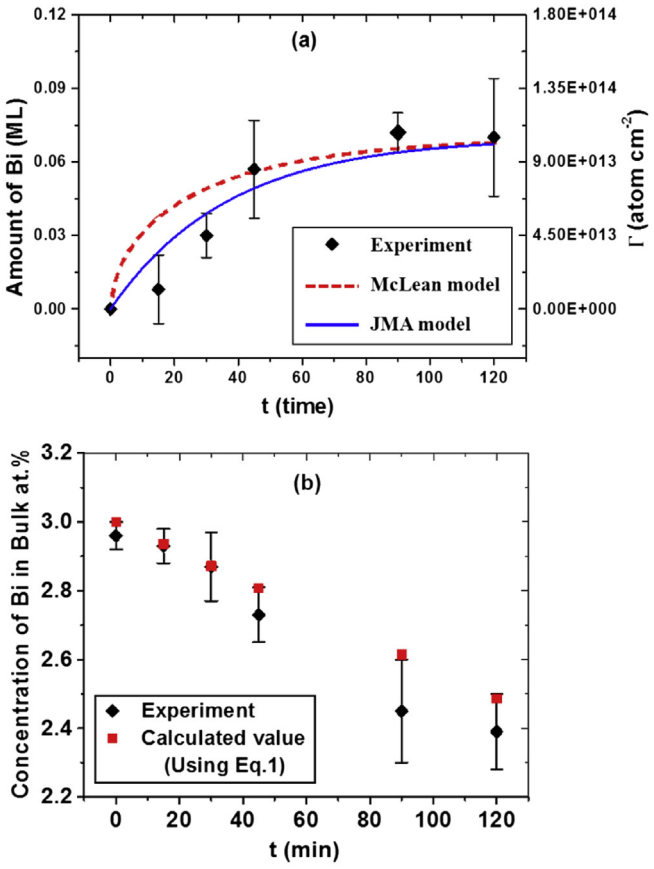

Fig. 6. a) The Gibbs-excess in Bi monolayer (or atom.cm^{-2}) units of GBs (average value) plotted versus time of isothermal annealing at 623 K. (b) Volume concentration of Bismuth for both measured and calculated values as function of time. Error bars mark error of mean value (σ/squrt(N)). N is the size the number of observed sample, and σ is the standard deviation.

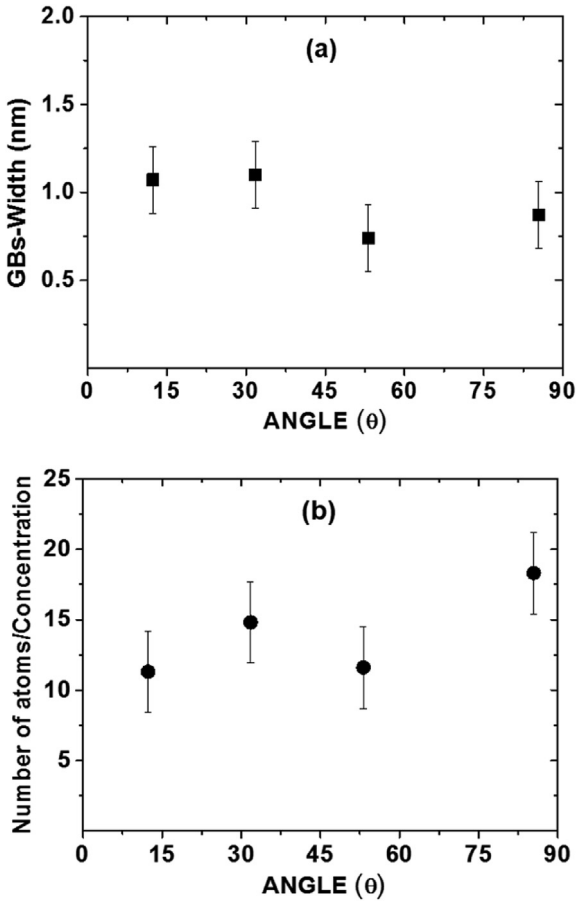

Fig. 7. Dependence of Bi concentration and width on GB orientation with respect to tip axis after 15 min annealing at T = 623 K, for (a) and (b) respectively.

variation of alloy compositions could trace the energy landscape around the GB for site occupancy by impurities.

ii) Segregation kinetics does not follow expected classical McLean behavior [33]. To describe the kinetics of segregation, McLean considered transport of impurities by volume diffusion from the neighbored grain volume towards the GB and derived:

$$\frac{C(t)-C(0)}{C(eq)-C(0)} = 1 - \exp\left[\frac{4D_B t}{(\alpha w)^2}\right] \cdot erfc\left(\frac{2\sqrt{D_B t}}{\alpha d}\right) \quad (2)$$

in which $C(t)$ and $C(eq)$ denote grain boundary segregation concentration at time t and in equilibrium after long annealing time, respectively. $C(0)$ represent grain boundary concentrations at the beginning which also approximates the bulk concentration. w is the thickness of the grain boundary, and $\alpha = C_{eq}/C_0$ is the segregation factor between GB and bulk, which is observed in our measurement to be $\alpha = 17$.

McLean's model has been widely used to estimate the time for reaching the equilibrium GB segregation [33]. However, in the kinetic equation of the McLeanean segregation, the width of the segregation zone plays no role. This means that the model neglects the time dependence of the volume concentration. Accordingly a more sensible evaluation is possible in this complex case, where both the maximum concentration and the GB width evolve with time. McLean originally considered an infinitesimally thin GB. We generalize his original formula by assuming the mean density of the grain boundary zone by the density of Ni, i.e. $\rho_{GB} = \rho_{Ni}$, one gets:

$$\Gamma(t) = \rho \cdot w(t) \cdot C_{GB}(t) \quad (3)$$

which is correct except a geometrical factor of the order one.

Combining Eqs. (2)–(3), another equation for the GB segregation of solute excess Γ can be described as:

$$\frac{\Gamma(t)}{\Gamma(eq)} = 1 - \exp\left[4D_B t \frac{\rho^2 C(0)^2}{\alpha^2 \Gamma(eq)^2}\right] .erfc\left[2\sqrt{D_B t}\ \frac{C(0)}{\Gamma(eq)}\right] \quad (4)$$

where $\Gamma(t)$ and $\Gamma(\infty)$ are the actual and saturation Gibbs-excess. This formula is not exactly equivalent with the one can be found in Reference [33], but contains an approximation $C_{GB}-C_b \approx C_{GB}$. Since the bulk composition is well below the scatter of the GB concentration we feel this approximation is justifiable. In Fig. 6(a), expected evolution of the GB segregation of solute excess Γ is

Table 1
Results of evaluated grain boundaries. In total 21 independent samples have been analyzed and evaluated for the present study.

t (min)	C_{max} (at. %)	Width (nm)	Γ (ML)
15	9.21 ± 1.7	0.93 ± 0.11	0.008 ± 0.014
30	20.22 ± 2.6	1.41 ± 0.19	0.03 ± 0.009
45	25.73 ± 3.2	1.56 ± 0.29	0.057 ± 0.02
90	32.21 ± 9.6	1.70 ± 0.24	0.072 ± 0.008
120	35.53 ± 3.5	1.65 ± 0.23	0.07 ± 0.024

plotted as a red dashed line. Apparently the agreement of Eq. (4) with measured data is remarkably poor. Since in initial stages, impurities can reach the GB after very short diffusion distances, the McLean concept will always predict fastest rate at the beginning which later can only slow due to the broadening of the diffusion zone to both sides of the GB. By contrast in our experimental data, we even notice an increase of segregation rate and an incubation time is at least indicated. We notice that this experimentally observed evolution can be formally described by a Johnson–Mehl–Avrami (JMA) kinetics processes:

$$\frac{\Gamma(t)}{\Gamma(eq)} = 1 - \exp(t/\tau)^m \quad (5)$$

where t is the annealing time. The incubation time τ is the time interval between the specimen reaching the annealing temperature and the time at which visible transformation occurs. The parameter « m » depends on the dimension or shape of grain (spherical-shape/3D → $m = 3$; disk-shape/2D → $m = 2$; rod-shape/1D → $m = 1$). If nucleation happens parallel with growth, for 3D spherical grain, m can be 4 or 5 under various circumstances. As indicated by the blue line in Fig. 6(a), a perfect match between the experimental data and JMA model is obtained (in case of $m = 2$), which suggests that attractive interaction between Bi atoms in the GB become important and may accelerate segregation in intermediate stages.

iii) Observed segregation kinetics is way faster than expected from volume diffusion. In spite of the bad agreement, we may use Eq. (4) at least for estimating the required diffusion coefficient to establish saturation after about 2 h of annealing. This leads to:

$$D_B \approx (2.16 \pm 0.48) \times 10^{-21} \ \ m^2 s^{-1} \quad (6)$$

In literature, we did not find any data for volume diffusivity of Bismuth in Nickel. But derived diffusion coefficient is certainly many orders of magnitude higher than Ni self-diffusion at this temperature (~10^{-28} m^2 s^{-1}, see Ref. [34]). This is a rather surprising result, since Bi is a substitutional impurity with an atomic radius even larger than that of the Ni host. Thus its diffusion velocity should be similar to the host. Furthermore, we carefully excluded any error in the annealing temperature as described before. Also supersaturation of vacancies, which may stem from the deposition process, can hardly be made responsible for the fast transport. In this case, we would expect in contrast to our observation the fastest process at the beginning which should slow down later when vacancy excess has escaped to the GBs.

Ni-/Cu–Bi alloys have been investigated intensively as theoretical model systems for GB segregation and embrittlement. There has been a debate on whether the Bi segregation into a Cu GBs is caused by an electronic effect [35] (i.e., impurity-induced electronic structure changes) or a strain effect linked with the large atomic size of Bi [36,37]. In Ref [36], authors showed that the creation of a Bi monolayer leads to a factor of 2–3 decrease in the work of separation of Cu GBs. However, a high-resolution scanning transmission electron microscopy (STEM) investigation revealed that if Ni polycrystal is in contact with a Bi–Ni liquid alloy, the Bi impurity atoms segregate into Ni GBs, by forming Bi layers in the GBs [38]. This finding calls for a reconsideration of the Bi embrittlement mechanism of Ni and Cu based super alloys models. In addition, Kang et al. [39], investigated the microscopic origin of the Bi-induced loss of cohesion of Ni and Cu GBs, by using first-principles calculations. They found that the Bi–Bi interlayer bonding is significantly weakened in the GBs, leading to a factor of 20–50 decrease in the GB, which has an important role in Bi-induced intergranular fracture of Ni and Cu polycrystals. Remarkably, Chang et al. [40] found in analogous studies of segregation in coarse-grained polycrystalline Cu similarly enhanced effective diffusion of Bi by Auger spectroscopy. Without any microscopic information, the authors proposed to explain this phenomenon by assuming formation of a Bi rich liquid at dislocation pipes, which would allow a fast transport of Bi atoms. In our microscopic data however, we were unable to observe any dislocations, e.g. by pipe-shaped segregation zones (and their presence is unlikely in such a fine Nanocrystalline material with ~10 nm average grain size). Thus, it is indicated that the application of the McLean concept to evaluate described segregation kinetics is in general doubtful and needs further clarification. Accordingly, the presence of the excess Bi in the GBs might create such a fast transport path.

Some investigations on the grain boundary embrittlement of Ni by liquid Bi have been reported [41–43]. It has been shown that liquid Bi easily penetrates along grain boundaries in solid Ni at 973 K. Although pure Bi is already in the liquid state at the studied temperature of 623 K, the observed continuous increase in width and composition with annealing time, the shape of the composition profile from GB core to the grain volume, as well as the limited maximum composition clearly demonstrate that a solid state segregation process takes place. In addition, grain boundary segregation of Bi in Ni polycrystals doped with Bi has been investigated by Chang and Huang [11]. Authors observed that the Bi segregation at GBs decreases with increasing temperature. Thus, it becomes obvious that Bi segregation weakens the Ni GB. It is generally supposed that GB weakening owing to impurity segregation can generate intergranular embrittlement. A well-known example is Hydrogen (H) induced Iron (Fe) or Ni embrittlement occurring from the GB strength reduction [44,45]. Another example is the weakening of a Ni GB with Sulfur (S) impurity, inducing the Ni intergranular embrittlement [46]. It was also shown that the embrittlement of Al alloy is associated with sodium (Na) or Calcium (Ca) GB segregation [47,48]. Furthermore, Ben Mostefa et al. [5] attributed the ductility drop in Fe–36Ni alloys to GB segregation of S and the ductility recovery at very high temperatures to dynamic recrystallization. In 2008, Chen et al. [12] proposed an interpretation of deformation by trace impurity Na in an Aluminium (Al) 5 wt% Magnesium (Mg) alloy. They reported that the ductility trough is mainly caused by sodium segregation-induced grain boundary embrittlement.

Based on the demonstrated segregation tendency shown in Fig. 6, it is probable that Bi segregation also induces the intermediate temperature embrittlement that was observed in the mechanically tested diluted alloy investigated in previous studies [6,13]. Thus, we further expect that the segregation-induced GB weakening causes the embrittlement, by considering that these GB's with reduced strength can act as a source of cracks or preferential crack paths. In addition, the measured final concentration is not far away from the ordered NiBi intermetallic phase. Therefore, we cannot exclude a possible hetero-nucleation in GBs. A careful analysis with different annealing sequences is essential to elucidate this question.

5. Conclusion

Grain boundary segregation of Bi in nanocrystalline Ni was investigated in detail by atom probe tomography. By chemical segregation, GBs are clearly marked and localized in 3D volume reconstructions, so that individual GBs are reliably identified and analyzed. So the Gibbsian excess and the width of the segregation layer were determined. It has been demonstrated that the

segregation width develops in correlation to segregation amplitude. Measured data is poorly described by the kinetic equation of McLean type equilibrium GB segregation. It is indicated that attractive interaction of Bi leads to unexpectedly high segregation rates and an incubation type kinetics better described by JMA concepts. Diffusivity of Bi in Ni and segregation amplitude were quantitatively determined. Our finding will stimulate supplementary investigations of impurity in GBs in other systems beyond the classical Langmuir–McLean type model and impurity-induced embrittlement mechanisms of metal GBs.

Acknowledgments

This work has been financially supported by the Deutscher Akademischer Austausch Dienst (DAAD), the Alexander von Humboldt Foundation (AvH), the National Natural Science Foundation of China (NSFC) (No. 51001011), the Deutsche Forschungsgemeinschaft (DFG) (No. SCHM 1182/9) and the Research Fund for the Doctoral Program of Higher Education of China (No. 20090006120011). The authors acknowledge Dr. Z. Balogh from Empa – Swiss Federal Laboratories for Materials Science and Technology, Switzerland, for invaluable scientific discussion and helpful comments.

References

[1] S. Neumeier, M. Dinkel, F. Pyczak, M. Göken, Nanoindentation and XRD investigations of single crystalline Ni–Ge brazed nickel-base superalloys PWA 1483 and René N5, Mater. Sci. Eng. A 528 (2011) 815–822.
[2] U. Krupp, W.M. Kane, C. Laird, C.J. McMahon, Brittle intergranular fracture of a Ni-base superalloy at high temperatures by dynamic embrittlement, Mater. Sci. Eng. A 387–389 (2004) 409–413.
[3] L.Z. He, Q. Zheng, X.F. Sun, G.C. Hou, H.R. Guan, Z.Q. Hu, Low ductility at intermediate temperature of Ni–base superalloy M963, Mater. Sci. Eng. A 380 (2004) 340–3478.
[4] F. Vogel, N. Wanderka, Z. Balogh, M. Ibrahim, P. Stender, G. Schmitz, J. Banhart, Mapping the evolution of hierarchical microstructures in a Ni-base superalloy, Nat. Commun. 4 (2013) 2955.
[5] L. Ben Mostefa, G. Saindrenan, M.P. Solignac, J.P. Colin, Effect of interfacial sulfur segregation on the hot ductility drop of Fe–36Ni alloys, Acta Mater. 39 (1991) 3111–3118.
[6] L. Zheng, G. Schmitz, Y. Meng, R. Chellali, R. Schlesiger, Mechanism of intermediate temperature embrittlement of Ni and Ni-based superalloys, Crit. Rev. Solid State Mater. Sci. 37 (2012) 181–214.
[7] G.A. Young, T.E. Capobianco, M.A. Penik, B.W. Morris, J.J. McGee, The mechanism of ductility dip cracking in nickel–chromium alloys, Weld. J. 87 (2008) 31–43.
[8] D.A. Woodford, Gas phase embrittlement and time dependent cracking of nickel based superalloys, Energy Mater. 1 (2006) 59.
[9] E.K. Athanassiou, R.N. Grass, N. Osterwalder, W.J. Stark, Preparation of homogeneous, bulk nanocrystalline Ni/Mo alloys with tripled vickers hardness using flame-made metal nanoparticles, Chem. Mater. 19 (2007) 4847–4854.
[10] Z. Miskovic, M. Jovanovic, M. Gligic, B. Lukic, Microstructural investigation of IN 939 superalloy, Vacuum 43 (1992) 709–711.
[11] L.S. Chang, K.B. Huang, Temperature dependence of the grain boundary segregation of Bi in Ni polycrystals, Scr. Mater. 51 (2004) 551–555.
[12] X.M. Chen, S.H. Song, L.Q. Weng, K. Wang, A consideration of intergranular fracture caused by trace impurity sodium in an Al–5 wt.% Mg alloy, Scr. Mater. 58 (2008) 902–905.
[13] L. Zheng, R. Chellali, R. Schlesiger, D. Baither, G. Schmitz, Intermediate temperature embrittlement in high-purity Ni and binary Ni(Bi) alloy, Scr. Mater. 65 (2011) 428–431.
[14] D. Briggs, M.P. Seah (Eds.), Practical Surface Analysis by Auger and X-ray Photoelectron Spectroscopy, second ed., Wiley, Chichester, UK, 1990.
[15] E.D. Hondros, M.P. Seah, S. Hofmann, P. Lejček, North-Holland: Amsterdam, in: R.W. Cahn, P. Haasen (Eds.), Physical Metallurgy, fourth ed., 1996, p. 1201.
[16] R. Kirchheim, Grain coarsening inhibited by solute segregation, Acta Mater. 50 (2002) 413–419.
[17] T. Chookajorn, H.A. Murdoch, C.A. Schuh, Design of stable nanocrystalline alloys, Science 337 (2012) 951–954.
[18] M.P. Harmer, The phase behavior of interfaces, Science 332 (2011) 182–183.
[19] J.K. Heuer, P.R. Okamoto, N.Q. Lam, J.F. Stubbins, Relationship between segregation-induced intergranular fracture and melting in the nickel–sulfur system, J. Appl. Phys. Lett. 76 (2000) 3403.
[20] J.Y.W. Seto, The electrical properties of polycrystalline silicon films, J. Appl. Phys. 46 (1975) 5247.
[21] L.-S. Chang, E. Rabkin, B.B. Straumal, B. Baretzky, W. Gust, Thermodynamic aspects of the grain boundary segregation in Cu(Bi) alloys, Acta Mater. 47 (1999) 4041–4046.
[22] L.-S. Chang, E. Rabkin, S. Hofmann, W. Gust, Kinetic aspects of the grain boundary segregation in Cu(Bi) alloys, Acta Mater. 47 (1999) 2951–2959.
[23] M. Kume, Honolulu, in: Proceedings of the 1st International Conference on Processing Materials for Properties, 1993, p. 597.
[24] V.M. Hutanu, V. Dolocan, in: Proceedings of SPIE-the International Society for Optical Engineering 4068, 2000, p. 149.
[25] M.K. Miller, A. Cerezo, M.G. Hetherington, G.D.W. Smith, Atom Probe Field Ion Microscopy, Clarendon Press, Oxford, 1996.
[26] P. Stender, Z. Balogh, G. Schmitz, Triple junction segregation in nanocrystalline multilayers, Phys. Rev. B 83 (2011) 121407 (R).
[27] Z. Balogh, P. Stender, M.R. Chellali, G. Schmitz, Investigation of interfaces by atom probe tomography, Metall. Mater. Trans. A 44 (2013) 4487–4495.
[28] H. Okamoto, Bi–Ni (Bismuth-Nickel), J. Phase Equilib. Diff. 33 (2012) 492.
[29] M.R. Chellali, Z. Balogh, L. Zheng, G. Schmitz, Triple junction and grain boundary diffusion in the Ni/Cu system, Scr. Mater. 65 (2011) 343–346.
[30] M.R. Chellali, Z. Balogh, H. Bouchikhaoui, R. Schlesiger, P. Stender, L. Zheng, G. Schmitz, Triple junction transport and the impact of grain boundary width in nanocrystalline Cu, Nano Lett. 12 (2012) 3448–3454.
[31] R. Sharghi-Moshtaghin, S. Asgari, The influence of thermal exposure on the γ' precipitates characteristics and tensile behavior of superalloy IN-738LC, J. Mater. Process. Technol. 147 (2004) 343–350.
[32] K. Gopinath, A.K. Gogia, S.V. Kamat, U. Ramamurty, Low cycle fatigue behaviour of a low interstitial Ni-base superalloy, Acta Mater. 57 (2009) 3450–3459.
[33] D. McLean, Grain Boundaries in Metals, Oxford University Press, London, 1957.
[34] H. Mehrer, Diffusion in solids metals and alloys, in: Landolt-Börnstein, New Series, vol. III/26, Springer Verlag, Berlin, Germany, 1990.
[35] G. Duscher, M.F. Chisholm, U. Alber, M. Rühle, Bismuth-induced embrittlement of copper grain boundaries, Nat. Mater. 3 (2004) 621–626.
[36] R. Schweinfest, A.T. Paxton, M.W. Finnis, Bismuth embrittlement of copper is an atomic size effect, Nature 432 (2004) 1008–1011.
[37] A.Y. Lozovoi, A.T. Paxton, M.W. Finnis, Structural and chemical embrittlement of grain boundaries by impurities: a general theory and first-principles calculations for copper, Phys. Rev. B 74 (2006) 155416.
[38] J. Luo, H. Cheng, K.M. Asl, C.J. Kiely, M.P. Harmer, The role of a bilayer interfacial phase on liquid metal Embrittlement, Science 333 (2011) 1730.
[39] J. Kang, G.C. Glatzmaier, S.-H. Wei, Origin of the bismuth-induced decohesion of nickel and copper grain boundaries, Phys. Rev. Lett. 111 (2013) 055502.
[40] L.-S. Chang, E. Rabkin, B.B. Straumal, B. Baretzky, W. Gust, Kinetics of the Bi segregation at grain boundaries in polycrystalline Cu, Mater. Sci. Forum 294–296 (1999) 585–588.
[41] K.V. Asl, J. Luo, Impurity effects on the intergranular liquid bismuth penetration in polycrystalline nickel, Acta. Mater. 60 (2012) 149–165.
[42] N. Marié, K. Wolski, M. Biscondi, Grain boundary penetration of nickel by liquid bismuth as a film of nanometric thickness, Scr. Mater. 43 (2000) 943–949.
[43] N. Marié, K. Wolski, M. Biscondi, Intergranular penetration and embrittlement of solid nickel through bismuth vapour condensation at 700 °C, J. Nucl. Mater. 296 (2001) 282–288.
[44] R.Q. Wu, A.J. Freeman, G.B. Olson, First principles determination of the effects of phosphorus and boron on iron grain boundary cohesion, Science 265 (1994) 376.
[45] W.T. Geng, A.J. Freeman, R. Wu, C.B. Geller, J.E. Raynolds, Embrittling and strengthening effects of hydrogen, boron, and phosphorus on a Σ5 nickel grain boundary, Phys. Rev. B 60 (1999) 7149.
[46] M. Yamaguchi, M. Shiga, H. Kaburaki, Grain boundary decohesion by impurity segregation in a nickel–sulfur system, Science 307 (2005) 393.
[47] H. Okada, M. Kanno, Hot ductility of Al–Mg and Al–Mg–Y alloys impaired by trace sodium, Scr. Mater. 37 (1997) 781.
[48] K. Horikawa, S. Kuramoto, M. Kanno, Intergranular fracture caused by trace impurities in an Al–5.5 mol% Mg alloy, Acta Mater. 49 (2001) 3981–3989.